Slow-light photonic crystal switches and modulators

Daryl M. Beggs*[a], Thomas P. White[a], Tobias Kampfrath[b], Kobus Kuipers[b], Thomas F. Krauss[a]
[a] School of Physics & Astronomy, University of St Andrews, KY16 9SS, UK;
[b] FOM Institute AMOLF, Science Park 113, 1098 XG Amsterdam, The Netherlands

ABSTRACT

We discuss the performance of slow-light enhanced optical switches and modulators fabricated in silicon. The switch is based on photonic crystal waveguides in a directional coupler geometry, and the dispersion of the device is engineered to allow a switching length as short as 5 μm and rerouting of optical signals within 3 ps. The 3 ps switching time is demonstrated using free carriers in the silicon generated by the absorption of a femtosecond pump pulse. The modulator is based on a Mach-Zehnder interferometer configuration, with photonic crystal waveguides in each arm to act as phase-shifters. A flat-band slow-light region has been engineered in the phase-shifters to provide an extinction ratio in excess of 15 dB over the entire 11 nm bandwidth of the modulator device.

Keywords: silicon, optical, switch, modulator, slow-light, photonic crystal, directional coupler, interferometer

1. INTRODUCTION

Optical switches and modulators are key components in next generation communications technologies. Firstly, future terabit per second tele-communications networks will increasingly operate all-optically, and optical switches will remove the bottleneck of the electro-optic conversion that is currently required for re-routing of signals. Secondly, as computer chips become massively parallel with multiple cores, on-chip optical communication becomes increasingly attractive as compared to the electronic equivalent. These technologies need cheap, reliable and compact optical switches and modulators that can be integrated on-chip. A further requirement is that they are made from silicon [1-11], ensuring CMOS compatibility.

Optical switching is an "easy" operation in III – V semiconductor systems, where large non-linear effects and refractive index modulation are available [12, 13]. However, in silicon photonics, switching is more difficult, owing to the weak non-linear effects and small refractive index changes available. The result is that devices tend to be either very long, or require high powers to operate.

One solution is to enhance the sensitivity of light to the small changes in refractive index available using a resonant effect [3]. Switching or re-routing light typically requires a π phase change between two optical paths or modes, a fact encapsulated in the equation $\Delta kL = \pi$, when L is the switching length and Δk is the wavevector difference between the two paths or modes. In order to reduce L, we engineer a device in which the Δk is large, even for the small change of refractive index available: such a condition is provided by a slow-light region.

Slow-light is a resonant effect. In periodic structures such as a photonic crystal, the forward and backward travelling components of the wave interfere to give a standing wave at the bandedge created by the periodicity of the structure. Just away from the bandedge, however, is a region of slow-light, where the envelope of the interfering backwards and forwards travelling components moves very slowly.

Here we report on progress toward the development of two slow light enhanced optical devices: a modulator and an optical switch. The modulator is described in section 3. It consists of a symmetric Mach-Zehnder interferometer (MZI) with slow-light photonic crystal waveguides in each arm. Switching is demonstrated using the thermo-optic effect via an integrated microheater. The MZI geometry, when combined with a photonic crystal phase shifter designed to have a large group index-bandwidth product, can provide modulation over appreciable bandwidths – here we demonstrate 11 nm – mitigating the usual trade-off between slow-light enhancement and bandwidth usual found when using resonant effects. The optical switch described in section 4 is based on two closely-spaced photonic crystal waveguides in a directional coupler (DC) geometry [11]. Switching was previously demonstrated using the thermo-optic effect, on a time-scale of 20 μs [14], but such a switching time is orders of magnitude too large for practical devices. Here, we report

Silicon Photonics V, edited by Joel A. Kubby, Graham T. Reed, Proc. of SPIE Vol. 7606, 76060N

on the switching time using a free-carrier effect to modulate the refractive index of the silicon (c.f. ref. [9]). Using a pump-probe experimental set-up, we demonstrate switching times as short as 3 ps [15, 16]. This time is not limited by the time-of-flight of the pulse, which is on a sub-ps timescale. On the contrary, the switch is bandwidth limited, in that a faster switching time can only be demonstrated with a shorter pulse, which would require more bandwidth than is available with this particular device.

The two device geometries presented here – MZI modulator and directional coupler – each have their own advantages. The MZI geometry allows a trade-off between the length and the phase-shift (a mechanism not available in the DC geometry) which is important in silicon where only small refractive index modulations are available. The DC geometry instead provides a strong interaction and therefore a very short length. This allows for more densely integrated circuitry but also (more importantly for future THz networks) shorter pulse transit times through the device and hence potentially faster operation and lower switching energies. Stability against temperature fluctuations (which will be important for on-chip applications) is more difficult to achieve in the DC geometry (possibly requiring active compensation), whereas the two balanced arms of the MZI make the geometry naturally temperature insensitive. The nature of the slow light enhancement in the MZI typically offers a bandwidth of $\Delta\lambda \approx$ 5-15 nm, while the DC is limited to around $\Delta\lambda \approx 1$ nm.

2. DISPERSION ENGINEERING

A silicon photonic crystal slab consists of a regular lattice of holes etched into a thin silicon membrane. By removing a single row of holes, as shown schematically in fig. 1 (d), a waveguide known as a W1 is formed with confinement in the plane of the slab light provided by the photonic band-gap, and vertical confinement provided by total internal reflection. This geometry has been studied extensively as it can support a single mode of even symmetry at frequencies within the bandgap of the photonic crystal.

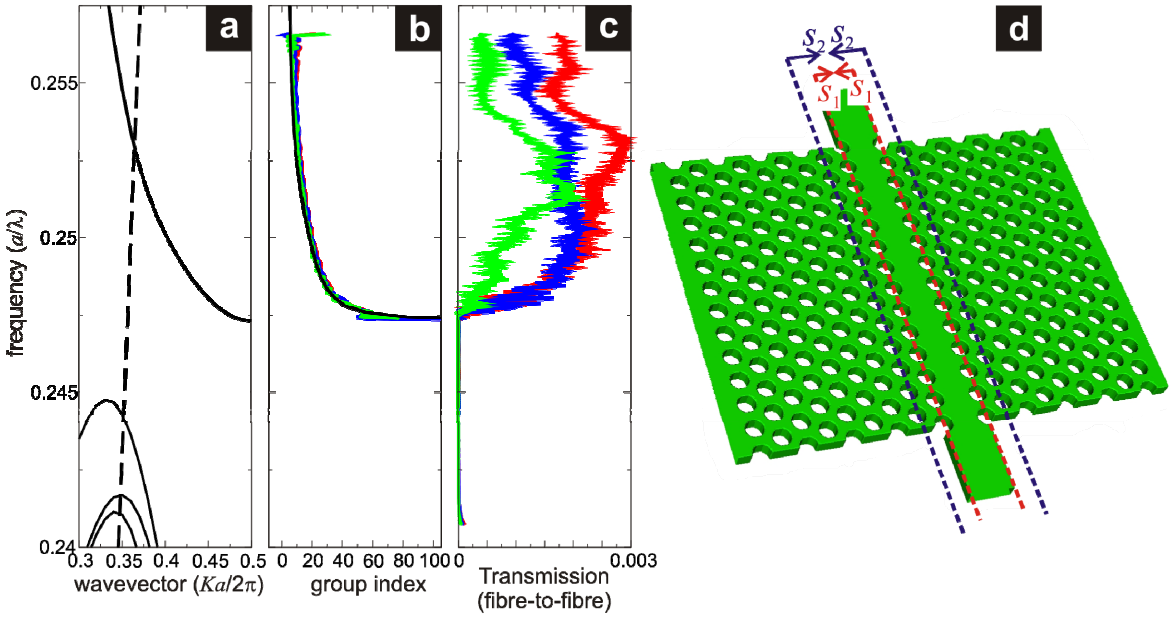

Figure 1. (a) Calculated dispersion relation for a W1 photonic crystal slab waveguide with a silica cladding. The W1 waveguiding mode is highlighted by the bold line, and the lightline of the silica cladding is shown by the dashed line. (b) Calculated (black line) and measured (red, green and blue lines) group index spectra for the same W1 system. (c) Measured transmission spectra for three different lengths of waveguides. (d) Schematic of the W1 photonic crystal slab waveguide, also showing the shift parameters s_1 and s_2 for the first and second rows of holes, which are used for engineering the dispersion, as described in the text.

The dispersion (k, ω) of the waveguide defect mode of interest is shown in fig. 1 (a). The group velocity is given by $n_g = d\omega/dk$, and so is represented by the slope of the dispersion curve. The group index calculated from the bandstructure is shown in fig. 1 (b) in addition to the measured group velocity [17] for three different lengths of W1 (20um, 30um and 80um). The excellent agreement between calculation and experiment, even for group indices in excess of 100, is

testament to the quality of the fabrication. Figure 1 (c) shows the measured transmission spectra of these three different length waveguides. As can be seen in fig. 1 (b), the group velocity dispersion is large, meaning the spectral components of any pulse will travel at different speeds, and the pulse will rapidly broaden. Thus we must engineer the dispersion in order to provide a region of "flat-band" slow-light, which is defined as a wavelength range where the group velocity dispersion is close to zero. A key metric for the performance of the flat-band slow-light region in devices is the group index-bandwidth product.

A variety of methods is available to engineer the waveguide dispersion to achieve flat-band slow-light, from altering the width of the waveguide [18-21] to changing the diameter of the holes near the defect [22, 23]. Here we have used the method described in ref. [20] – the first two rows of holes are shifted inwards by a distance s_1 (for the first row) and s_2 (for the second row). This scheme avoids the need for nanometre control the hole size, which is difficult [24], and instead uses nanometre control of the hole position, which is relatively easy task in electron-beam lithography. Scanning the parameters s_1 and s_2 provides a systematic way of designing waveguides with high group index-bandwidth product. Figure 2 shows the measured group index from a series of these designs with different shift parameters s_1 and s_2. Each waveguide has a region of flat-band slow-light, indicated by the shaded bands, where the group index is assumed "constant" if it varies by less than 10% throughout the entire band. In all cases, the normalised group index-bandwidth product $n_g.\Delta\lambda/\lambda_0$ is approximately 0.3, but the design is flexible enough to allow the systematic trade-off between n_g and $\Delta\lambda$ as is required by particular device designs.

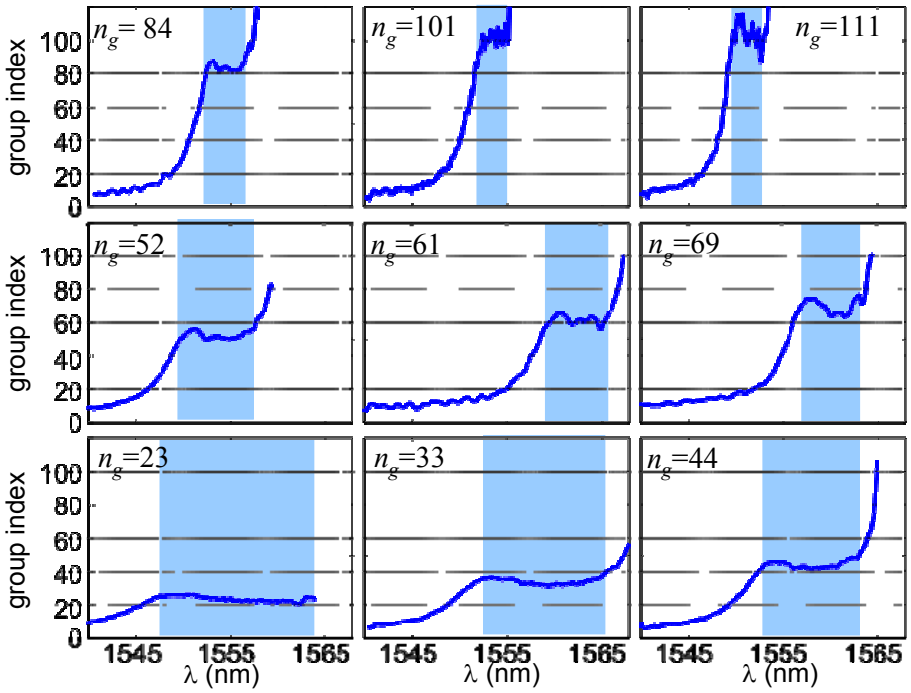

Figure 2. Group index measurements of photonic crystal waveguides that have been designed to have regions of flat-band slow-light of constant group index-bandwidth products, but differing group indices (as indicated). The shaded bars represent the wavelength range within which the group index varies by less than 10%.

3. PHOTONIC CRYSTAL MODULATOR

3.1 Modulator design and fabrication

The modulator design consists of a symmetric Mach-Zehnder interferometer with a dispersion-engineered photonic crystal waveguide in each arm, as shown in fig. 3. The thermo-optic effect in silicon is used to provide the phase-shift in one of the arms via an integrated microheater. The photonic crystal waveguides are designed to have a constant group index of 28 over a large bandwidth of approximately 13 nm. The entire structure is covered with a silica cladding (highlighted in the cross-section of fig. 3 (b)), which, although it reduces the index contrast, improves CMOS compatibility and provides a spacer layer to isolate the optical modes from the microheaters. The microheaters are

fabricated from 5 μm wide, 80 nm thick, strips of nickel that act as resistive elements when a current is applied, causing heat to be dissipated into the device.

The fabrication closely follows that in refs. [25] and [26] (c.f. the fabrication of the switch in ref. [14]). A SOITEC silicon-on-insulator wafer with 220 nm of silicon on a 2 um thick buried oxide layer is spun with 400 nm layer of ZEP-520A (Zeon Chemicals) to be used as an electron-beam resist. The ZEP-520A is patterned with the MZI and PhC designs using electron-beam lithography, and this pattern is transferred to the silicon layer by reactive ion etching with a SF_6/CHF_3 gas mixture. The holes making up the PhC waveguide and the MZI design can be seen in fig. 3 (c) and (d) respectively. A silica cladding is then deposited using the spin-on-glass FOx-14 (commercially available from Dow-Corning), which leaves a 600 nm layer after hard-baking at 400°C for 3 hours. An integrated nickel microheater is then added over one of the PhC phase-shifters using a photo-lithography, evaporation deposition, and lift-off procedure. A micrograph of the final device is shown in fig 3 (a).

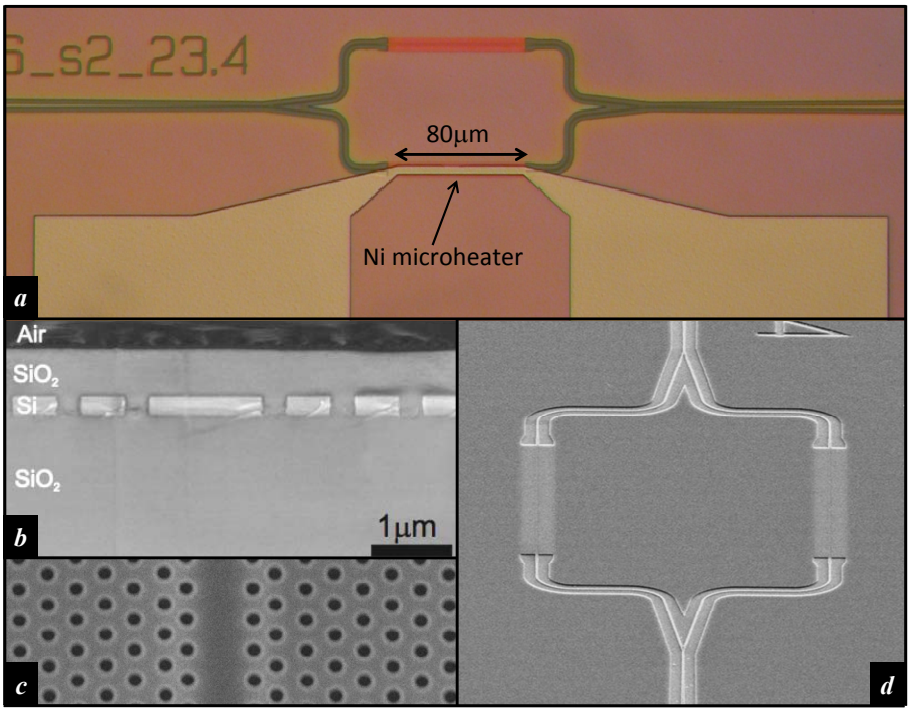

Figure 3. Fabrication of the modulator design. (a) Micrograph of the finished device. The 80 μm short PhC phase-shifters can be seen in each arm of the MZI. The nickel microheater and electrical contact pads can also be seen. (b) SEM of a cross-section through the PhC phase-shifters. The silicon guiding layer is covered with an oxide cladding, which is seen to fill the holes. (c) A close-up of the PhC waveguide. The shift of the first two rows of holes adjacent to the waveguide (which is used to engineer the dispersion) can be seen. (d) An overview of the device design.

The silicon layer has a thermo-optic coefficient of $\Delta n = 1.8 \times 10^{-4}$ K^{-1}, and so its refractive index increases with temperature, shifting the dispersion of the photonic crystal waveguide mode to lower frequencies. This shift (see fig. 4 (inset)) induces a phase-shift between the two arms of ΔkL – a phase shift of π is required to switch the signal from on to off. The advantage of the slow-light design is now apparent – it allows a greater phase shift per unit length of the waveguide, meaning the overall length of the device can be smaller. As shown in fig. 4 (inset), the shift in wavevector when the microheater is on is $\Delta k = \Delta n\ \omega 0\ S$, where $S = n_g/n$ is the slow-down factor, Δn is the change of refractive index and ω_0 is the frequency. Thus the length required for a π-phase shift is reduced by a factor S in our slow-light designs. In the example here, a phase-shifter 80 μm long was required to operate with an index change of approximately 10^{-3}. The traditional trade-off of the slow-down factor with bandwidth is some-what mitigated by our use of PhC waveguides with a large group index-bandwidth product. Figure 4 shows the measured group-index curves for the photonic crystal phase-shifters.

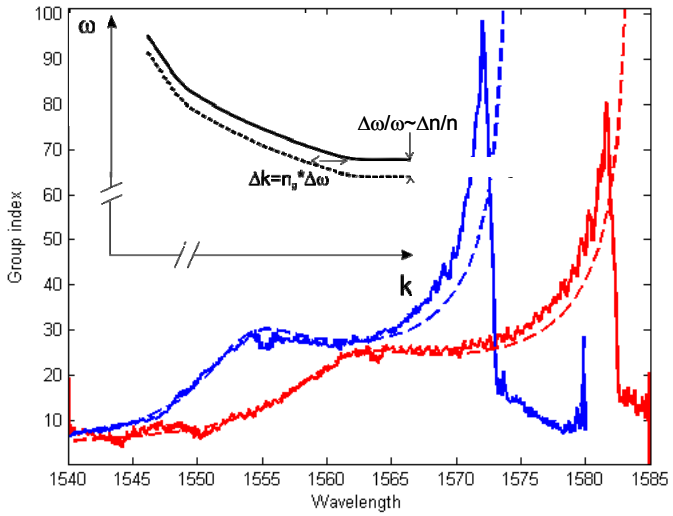

Figure 4. Measured (solid lines) and calculated (dashed lines) group index spectra for the dispersion engineered PhC waveguides to be used a phase-shifters in the modulator device. The flat-band slow-light region can be identified at approximately $n_g = 30$.

3.2 Modulator performance

The transmission spectra of the modulator devices were measured using a broadband (1520 – 1620 nm) amplified spontaneous emission (ASE) source and an optical spectrum analyser (OSA) in an end-fire configuration. The transverse electric (TE) polarisation – electric field in the plane of the silicon slab – was selected by the use of a polarising beam splitter cube. The integrated micro-heaters were contacted on the chip using needle probes, and the transmission spectra taken as function of the electrical power delivered to the heater. The optical alignment of the device in the end-fire set-up must be maintained to sub-micron accuracy over the ~20 minute timescale of the experiment. The results are shown in fig. 5.

Figures 5 (a) and (b) show the theoretical and measured transmission spectra as a function of the refractive index change, Δn, of the PhC phase-shifter (theoretical) or the electrical power delivered to the micro-heater (experimental). The colour bar shows the transmission in dB, and the scale covers a range of 10 dB. It is clear that the measurements qualitatively match the expected performance of the switch, once the power axis is calibrated to a change in refractive index.

Figure 5 (c) shows the transmission as a function of the electrical power of the microheater at a wavelength of 1581 nm (the cut shown by the solid line in (b)). It can be noted that the first peak in transmission occurs at a power of approximately 9 mW (as opposed to the expected 0 mW). This indicates that before the microheater is turned on, the MZI is slightly unbalanced; this unbalancing being corrected by 9mW of heating. This unbalancing could be due to fabrication tolerances meaning that the arms are not quite equal, or the metal for the heater causing a small disturbance of the optical mode, despite being ~600 nm away on top of the silica buffer layer.

The power required for the π-phase change needed to switch the modulator from on to off is $P_\pi = 17$ mW, and the measured modulation depth is an impressive 20dB. The broadband operation of our modulator design can also be seen from fig. 5 (b) – we have measured a bandwidth of 11 nm from 1576 nm to 1587 nm (marked by the dashed lines) over which the entire band is modulated at the same time. Figure 5 (d) shows the average transmission over the 11 nm bandwidth as a function of the electrical power: remarkably, the extinction ratio exceeds 15dB over the whole 11 nm.

In the present device the insertion efficiency is relatively low, with a measured insertion loss of 8-12dB. The high insertion loss can be explained by fabrication errors in the junction and photonic wires, and does not represent a limit to our device design. In fact, the PhC phase-shifters are expected to have a total loss of < 0.5 dB, given a loss per unit length in the flat-band slow-light region of the PhC phase-shifters of 30-40dB/cm [27].

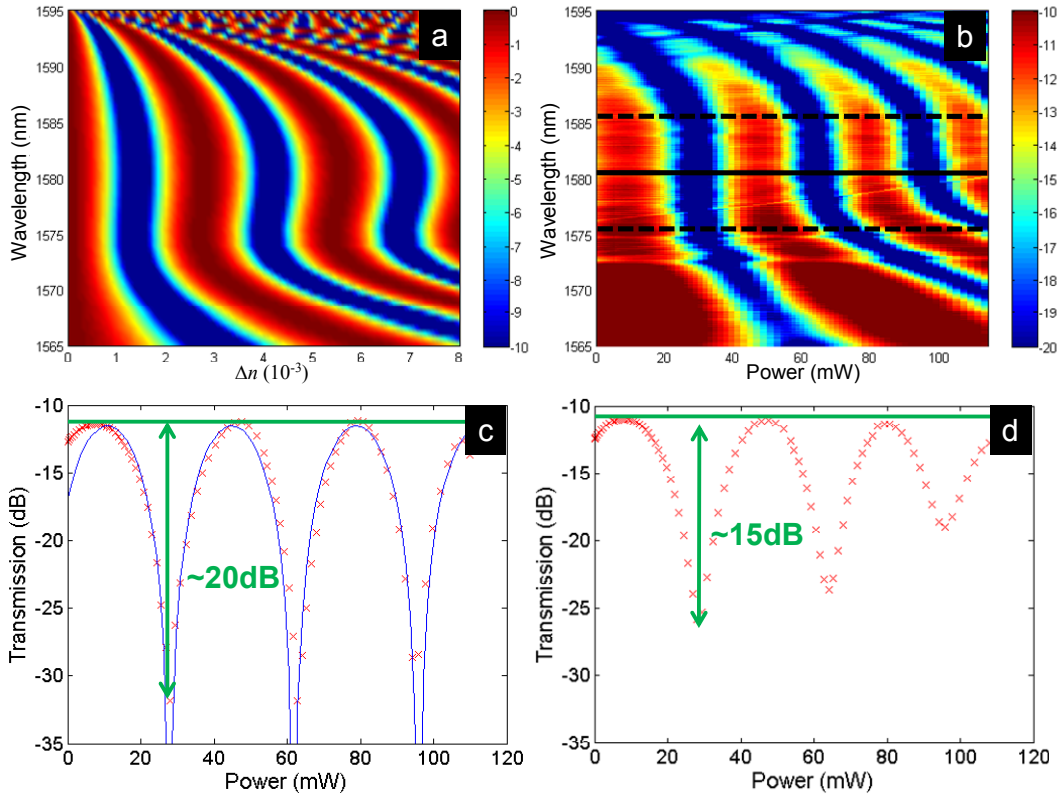

Figure 5. (a) Theoretical transmission spectra of MZI modulator as a function of Δn, the change of refractive index of the silicon in one of the PhC phase-shifters. The colour bar gives the transmission in decibels. (b) Measured transmission spectra of MZI modulator as a function of the electrical power delivered to the integrated microheater. The dashed lines represent the limits of the 11 nm bandwidth, defined by the spectral region of flat-band slow-light in the dispersion engineered PhC phase-shifters. The colour bar gives the transmission in decibels. (c) Measured (red crosses) and calculated (blue lines) transmission as a function of electrical power delivered to the microheater at a wavelength of 1581 nm, as marked by the solid line in (b). (d) Average transmission over the 11 nm bandwidth as indicated by the dashed lines in (b).

In table 1 we have compared the performance of our modulator device to another state-of-the-art thermo-optic modulator with PhC-based design [28] and an electro-optic modulators with a conventional waveguide-based design [8, 29]. Ref. [28] used the thermo-optic optic effect in silicon by passing a current directly through the doped-silicon waveguides and achieved fast (100ns) and efficient (2mW electrical power) operation. However, at less than 0.5 nm, the optical bandwidth would limit the speed of the device to under 60Ghz. In contrast, our device, with its 11 nm bandwidth, could still operate even at data rates in excess of 1 THz.

Table 1. Comparison of silicon optical modulators.

	Intel 2005 [29]	IBM 2005 [28]	IBM 2007 [8]	This work
Modulation	Electro-optic	Thermo-optic	Electro-optic	Thermo-optic
Insertion loss	10dB	1-3dB (?)	12dB	8-12dB
Extinction (low freq)	~16dB	~20dB	6-10dB	20dB
Δn			4×10^{-3}	$1\text{-}2 \times 10^{-3}$
$V\pi.L\pi$ (V.cm)	3.3		3.6×10^{-2}	7.5×10^{-3}
$P\pi$ (mW)		~2		17
Optical bandwidth		<0.5nm		>10nm

Although we have not directly measured the speed of our device, we expect it to be similar to the switch in ref. [14] at around 20 μs. Clearly, this is orders of magnitude too slow for practical deployment. One solution is to use the electro-optic effect – the change in refractive index that accompanies a change in the density of charge carriers – as a modulation method, rather than the thermo-optic effect. The carriers would be injected (or depleted) via an integrated p-i-n doped structure, with the PhC phase shifter fabricated within the intrinsic region. With suitably designed contacts, the small size of the PhC phase shifter would afford an extremely small capacitance, enabling high speed operation. In fact, GHz operation for a similar p-i-n junction integrated with a PhC nano-cavity has recently been demonstrated [30].

4. PHOTONIC CRYSTAL SWITCH

4.1 Switch design and fabrication

An alternative geometry for switching or modulating an optical signal is a directional coupler consisting of two identical waveguides placed in close proximity to one another. Here we present a photonic crystal directional coupler that uses slow light to achieve a very short coupling length and demonstrate switching times of 3 ps. The photonic crystal DC switch is shown in fig 6 (a) and schematically in fig 7 (a). It consists of two PhC waveguides placed close enough that the optical modes in each waveguide overlap and interact with each other. As with a conventional directional coupler, the composite system supports two supermodes, one with even and the other with odd symmetry. Due to the difference in wavevector of these two modes, light in the system will couple from one waveguide to the other after a relative phase shift of π has occurred. The switching length is thus $L = \pi / \Delta k$. Similar to the case of engineering the dispersion for the modulator above, we want to engineer a large Δk such that the switching length L will be small. The problem is that available modulation of refractive index is small, so we need a large Δk for a small Δn – such a condition is provided by a slow-light region.

The dispersion of a photonic crystal waveguide can be engineered by adjusting the holes near the waveguide [20, 22]. Our scheme to engineer the dispersion follows ref. [31] – the sizes of the holes of the first two rows closest to the waveguide are altered. The final design geometry can be seen in fig. 6. Figure 7 (b) shows the resulting dispersion relation of the coupled modes in the central switch region. Also included in the design are interface regions of a slightly different dispersion to the switch region. The interfaces efficiently couple the fast light from the input/output slab waveguides into/out of the engineered modes of the switch. This is achieved by increasing the lattice constant of the switch region along the direction of the waveguide only, in order to lower the frequency of the interface bands with respect to the switch bands and light with a frequency designed to switch will experience a fast mode.

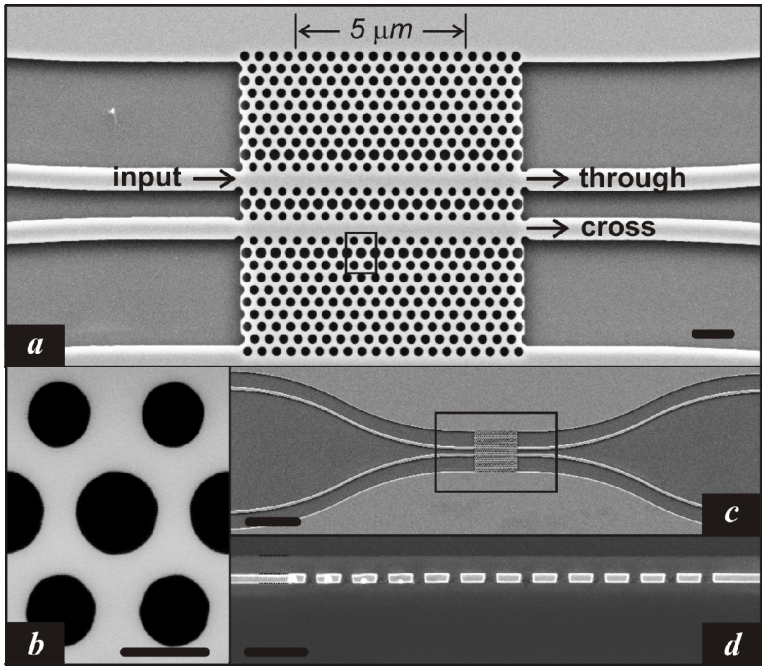

Figure 6. (a-c) Scanning electron micrographs of the directional coupler switch. (a) The switch design uses two closely-spaced PhC waveguides in a directional-coupler geometry. Scale bar 1um. (b) Close-up of holes in the PhC. Scale bar 300nm. (c) Overview of the chip layout. S-bends are used to separate the access waveguides. Scale bar 10um. (d) Cross-section through the PhC switch after silica infilling. Scale bar 1um.

The performance of the switch is dependent on the fidelity of the hole size control. If the hole diameter deviates from the design specification by more than 8-10 nm, the flat slow-light region of the engineered dispersion will broaden in frequency, resulting in an increased switching energy and decreased bandwidth. Because of this, we have developed nanometre control of the hole sizes in the waveguides [24]. We estimate that a 1% increase in electron-beam dose when patterning the resist results in a 1 nm increase of the final hole radius [24], providing us with a scheme to fine-tune the hole sizes between fabrication runs.

Our devices are fabricated in the silicon-on-insulator material system in a similar way to the fabrication of the modulator device described in section 3. For more details, see ref. [11] and [14].

4.2 Switch performance

Switching has been demonstrated in a 5 μm long device using a refractive index modulation of just $\Delta n = 4 \times 10^{-3}$. This is almost a 40 times reduction in length compared to switches designed to operate with a similar Δn [28]. The total footprint of the device (including interface regions) is just 10 μm × 10 μm, offering the possibility for densely integrated networks.

The insertion loss is around 1dB, which is comparable to that of the simple W1 photonic crystal waveguide. The bandwidth is 1-2 nm, which compares favourably with other switches and modulators based on resonant effects (for example, high-Q nano-cavities [10]).

4.3 Ultrafast measurements

In order to study the ultrafast dynamics of the switch, a pump-probe experiment was conducted. The silicon membrane is illuminated from above, as shown schematically in fig. 7 (a), by pump pulses of 100 fs duration, centre wavelength 800 nm, and a repetition rate of 80 MHz from a Ti:sapphire laser oscillator. The pumped silicon area has a diameter of around 20 μm, such that the absorption of each pump pulse generates a homogeneous electron-hole plasma in the silicon. The instantaneous transmission from both the through and cross-ports is then measured using probe pulses of a centre wavelength of 1486 nm (chosen as the wavelength at which the switch was designed to operate) and a bandwidth of 1.2 nm (which corresponds to a pulse duration of 2.8 ps). The probe pulses are derived from the same laser source as the pump, using an optical parametric oscillator and a grating-based reflexive pulse shaper [32].

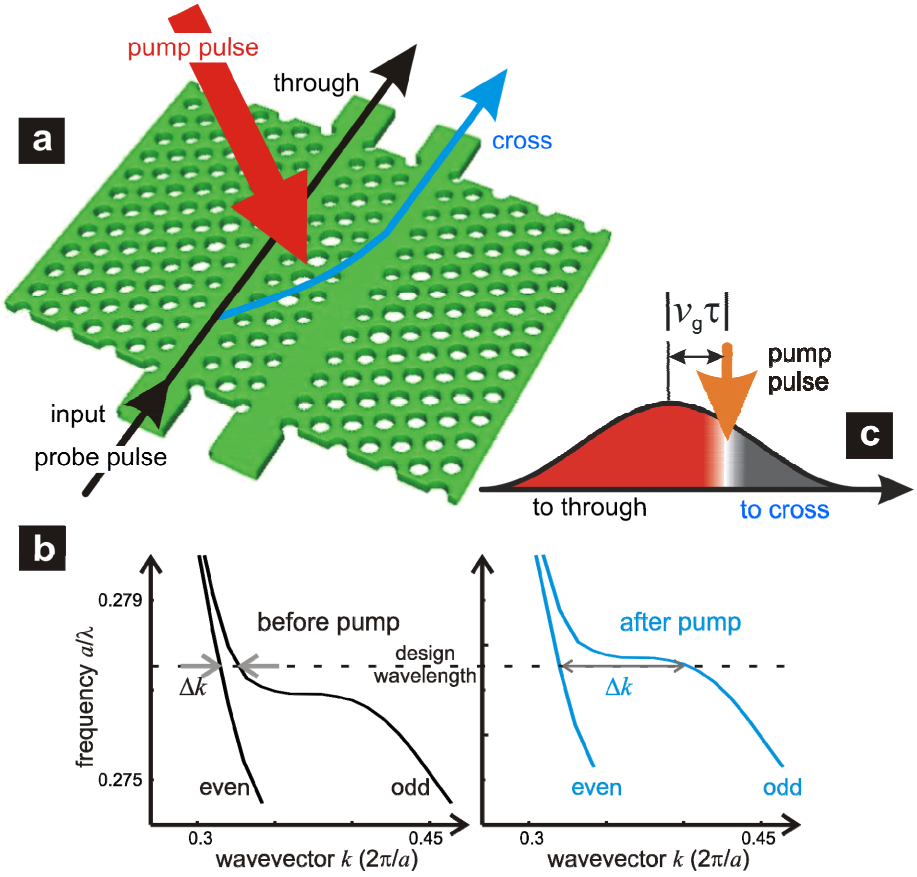

Figure 7. (a) Schematic of the device and the pump-probe experimental set-up. (b) Dispersion relation of the even and odd coupled supermodes of the device in the switching region, both before and after arrival of the pump pulse. (c) Illustration of the rerouting process for delays around $\tau = 0$. Probe light arriving before (after) the pump pulse exits the device at the through (cross) output ports.

The probe pulses are delayed with respect to the pump pulses (here a delay of zero means that the pump and probe arrive together at the centre of the device) and then coupled to the input port of the device. The transmitted probe pulse is collected by a lensed fibre at either the through or cross port and analysed by an optical spectrum analyzer.

Figure 8 (a) and (b) respectively show the probe intensity that reaches the through and cross-ports as a function of the wavelength and pump-probe delay. For delays $\tau < -2$ ps, the probe pulse arrives before the pump, encounters the device in its ground state and is detected at the through port, with no intensity being switched to the cross-port. For delays $\tau > 2$ ps, the probe pulse arrives after the pump, encounters the device in the switching state, and is coupled to the cross-port. Figure 8 (c) shows the total probe power arriving at the through and cross-ports. Note that over 80% of the power is switched between ports in a window of less than 3 ps. The power at the output ports can be very accurately modelled using

$$\text{through-port probe power} \propto \int_{\tau}^{\infty} I(t)dt \tag{1}$$

and

$$\text{cross-port probe power} \propto \int_{-\infty}^{\tau} I(t)dt\,. \tag{2}$$

where $I(t)$ is the intensity of the incident 2.8 ps Guassian probe pulse centred at $\tau = 0$. This leads to the conclusion that the 3 ps switching time is solely limited by the duration of the probe pulse, and not the time-of-flight of the pulse through

the device, in contrast to alternative (longer) designs [3, 33, 34]. Therefore the ultimate limitation on the switching time of our device is the bandwidth of the pulses that can be accommodated.

The above can be understood in terms of the probe-pulse being cut into two separate pulses when τ is around zero, as illustrated in fig. 7 (c). Upon arrival of the pump pulse, the leading edge of the probe pulse has already exited the device via the through port. The trailing edge of the pulse is yet to enter the device, and will thus encounter the switching state and be directed to the cross-port. The remaining part of the probe pulse (that part actually inside the switching region on arrival of the pump) can be neglected, as the transit time of the pulse (0.2 ps) is much smaller than its total duration (2.8 ps).

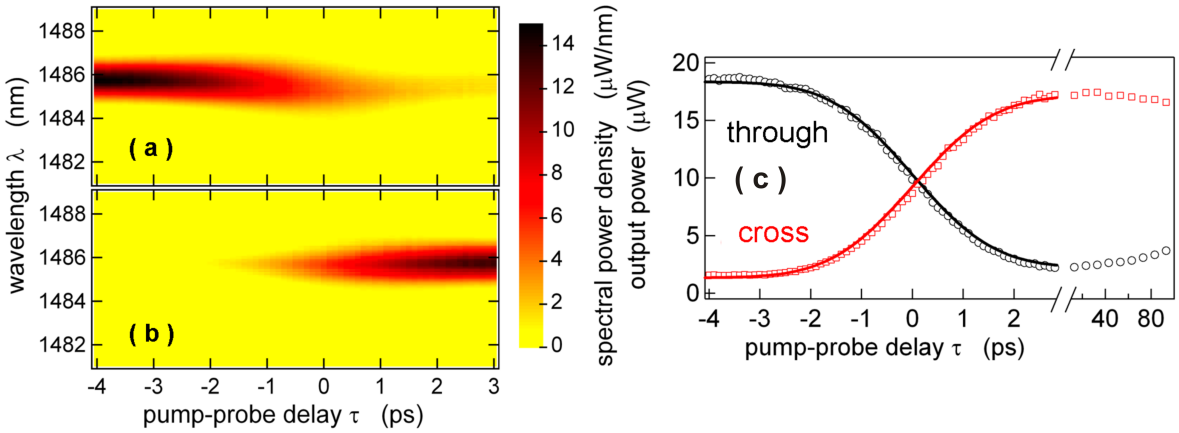

Figure 8. Experimental data demonstrating the ultrafast rerouting of light. (a) Spectra of the probe pulses arriving at the through port as a function of the pump-probe delay time τ. (b) Same for the cross port. (c) Total power in the probe beam arriving at the through-port (black circles) and cross-port (red squares) as a function of τ. Lines are calculations based on eqs. (1) and (2).

Figure 8 also shows the dynamics of the device on longer time-scales. It is apparent that the relaxation time of the switch after a switching event back to its ground state is on very much longer time scales than the 3 ps switching time. In fact, the device takes around 400 ps to relax, which is governed by the time taken for the free carriers in the electron-hole plasma to recombine. This time could be shortened (for example) by doping the silicon in a p-i-n configuration – the resulting diode could then be operated in reverse bias, enabling the fields to "sweep out" the generated free carriers on shorter time scales. Figure 9 (a) shows a photonic crystal switch aligned in the intrinsic region of a p-i-n junction, which is work in progress. The graph in fig. 9 (b) shows the measured electrical characteristics of the p-i-n junction; ultrafast characterisation is in progress.

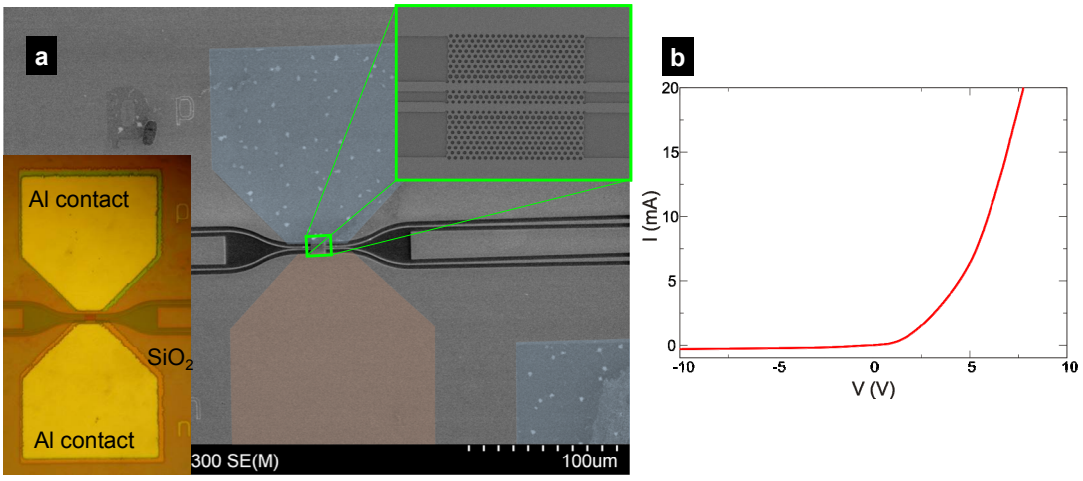

Figure 9. (a) p-i-n doping structure with a PhC directional coupler switch aligned in the intrinsic region. (b) Electrical characterization of p-i-n structure.

5. CONCLUSION

We have described the design, fabrication and characterisation of a silicon photonic crystal optical switch based on a directional coupler geometry as well as a Mach-Zehnder type modulator. Both designs have used slow-light photonic crystal slab waveguides to provide resonant enhancement.

The Mach-Zehnder modulator used flat-band slow-light photonic crystal waveguides placed in each arm to be used a phase shifters. An integrated microheater was used to actuate the device via the thermo-optic effect. The phase-shifters were shown to have a large group index-bandwidth product, which allowed them to be just 80 μm short whilst still providing over 15 dB extinction ratio over a large bandwidth of 11 nm. Thus the usual trade-off of severe bandwidth reduction associated with resonant enhancement has been mitigated.

The directional coupler switch featured a slow-light design which enabled a very short device length of just 5 μm. Using ultrafast pump-probe measurements, we demonstrated switching times as short as 3 ps, which (given the short transit time in our 5 μm device) is limited only by the duration of the input pulse. Therefore the speed of the switch is shown to be bandwidth limited – faster switching times may only be shown by increasing the bandwidth of the device and using shorter pulses.

These devices demonstrate the significant enhancements provided slow light for achieving ultracompact, low power optical devices and we believe that photonic crystal slow light enhancement provides an excellent compromise between size and switching power limitation on the one hand and bandwidth availability on the other, in contrast to cavity-based solutions. The designs presented here are fully CMOS compatible and can be used with high speed modulation approaches based on electro-optic effects. Work on both of these aspects is in progress to demonstrate high speed optical switching and modulation in an integrated on-chip geometry.

REFERENCES

1. Reed, G. T. and Png, C. E. J, "Silicon optical modulators", Materials Today pp. 40-50 January 2005.
2. Reed, G. T., "The optical age of silicon," Nature 427, 595-596, (2004).
3. Almeida, V. R., Barrios, C. A., Panepucci, R. R. and Lipson, M. "All-optical control of light on a silicon chip," Nature 431 1081 (2004).
4. Liu, A., Liao, L., Rubin, D., Nguyen, H., Ciftcioglu, B., Chetrit, Y., Izhaky, N. and Paniccia, M., "High-speed optical modulation based on carrier depletion in a silicon waveguide," Opt. Express 15(2) 660-668 (2007)
5. Liu, A., Jones, R., Liao, L., Samara-Rubio, D., Rubin, D., Cohen, O., Nicolaescu, R. and Paniccia, M., "A high speed silicon optical modulator based on a metal-oxide-semiconductor capacitor," Nature 427 615-618 (2004).
6. Xu, Q., Schmidt, B., Pradhan, S. and Lipson, M., "Micrometre-scale silicon electro-optic modulator," Nature 435, 325-327 (2005).
7. Lipson, M., "Silicon photonics: the optical spice rack," Electron. Lett., 45 (12), doi: 10.1049/el.2009.1232, (2009)
8. Green, W. M. J., Rooks, M. J., Sekaric, L., and Vlasov, Y. A., "Ultra-compact, low RF power, 10 Gb/s silicon Mach-Zehnder modulator,"Opt. Express 15 (25) 17106 (2007).
9. Vlasov, Y., Green, W. M. J., and Xia, F., "High-throughput silicon nanophotonic wavelength-insensitive switch for on-chip optical networks," Nature Photonics 2, 242-246 (2008)
10. Notomi, M., Shinya, A., Mitsugi, S., Kira, G., Kuramochi, E. and Tanabe, T., "Optical bistable switching action of Si high-Q photonic-crystal nanocavities," Opt. Express 13 2678-2687 (2005).
11. Beggs, D. M., White, T. P., O'Faolain, L. and Krauss, T. F., "Ultracompact and low power optical switch based on silicon photonic crystals," Opt. Letters 33 (2) 147 (2008).
12. Ibrahim T. A., et al., "All-optical switching in a laterally coupled microring resonator by carrier injection," Photonics Technol. Letters 15, 36-38 (2003).
13. Van, V., Ibrahim, T. A., Ritter, K., Absil, P. P., Johnson. F.G., Grover, R., Goldhar, J. and Ho, P. T., "All-optical non-linear switching in GaAs-AlGaAs microring resonators," Photonics Technol. Lett. 14 74-76 (2002).
14. Beggs, D. M., White, T. P., Cairns, L., O'Faolain, L. and Krauss, T. F., "Ultrashort photonic crystal optical switch actuated by a microheater," Photonics Technol. Lett. 21 (1) 24 (2009).
15. Kampfrath, T., Beggs, D. M., White, T. P., Burresi, M., van Oosten, D., Krauss, T. F. and Kuipers, L., "Ultrafast re-routing of light via slow modes in a nano-photonic directional coupler," Appl. Phys. Lett., 94 (24) 241119 (2009).

16. Kampfrath, T., Beggs, D. M., Krauss, T. F. and Kuipers, L., "Full characterization of ultrafast nano-photonic devices," Opt. Letters 34 (21) 3418-3420 (2009).
17. Gomez-Iglesias, A., O'Brien, D., O'Faolain, L., Miller, A. and Krauss, T. F., "Direct measurement of the group index of photonic crystal waveguides via Fourier transform spectral interferometry," Appl. Phys. Lett. 90, 261107, (2007).
18. Petrov A.Y. and Eich M., "Zero dispersion at small group velocities in photonic crystal waveguides", Appl. Phys. Lett., 85 (21) 4866-4868 (2004).
19. Settle, M. D., P.Engelen, R. J., Salib, M., Michaeli, A., Kuipers, L. and Krauss, T. F., "Flatband slow light in photonic crystals featuring spatial pulse compression and terahertz bandwidth" Opt. Express 15 (1): 219-226 (2007)
20. Li, J., White, T. P., O'Faolain, L., Gomez-Iglesias, A. and Krauss, T. F., "Systematic design of flat band slow light in photonic crystal waveguides", Optics Express 16 6227-6232 (2008).
21. Brosi, J.-M., Leuthold, J. and Freude, W., "Microwave-frequency experiments validate optical simulation tools and demonstrate novel dispersion-tailored photonic crystal waveguides," J. Lightwave Technol. 25, 2502-2510 (2007)
22. Frandsen, L. H., Lavrinenko, A. V., Fage-Pedersen, J. and Borel, P. I., "Photonic crystal waveguides with semi-slow light and tailored dispersion properties," Opt. Express 14 9444-9450 (2006).
23. Kubo, S., Mori, D. and Baba T., "Low-group-velocity and low-dispersion slow light in photonic crystal waveguides," Opt. Letters 32, 2981-2983 (2007)
24. Beggs, D. M., O'Faolain, L., and Krauss, T. F., "Accurate determination of the functional hole size in photonic crystal slabs using optical methods," Photonics and Nanostructures – Fund. and Appl. 6, 213-218 (2008).
25. O'Faolain, L., Yuan, X., McIntyre, D., Thoms, S., Chong, H., De la Rue, R. M. and Krauss, T. F., "Low-loss propagation in photonic crystal waveguides," Electron. Lett. 42 (25) 1454-1455 (2006).
26. White, T. P., O'Faolain, L., Li, J., Andreani, L. C. and Krauss, T. F., "Silica-embedded silicon photonic crystal waveguides," Opt. Express 16 (21) 17076-17081 (2008)
27. Krauss, T. F, O'Faolain, L., Schulz, S., Beggs, D. M., Morichetti, F., Canciamilla, A., Melloni, A., Lalanne, P., Samarelli, A., Sorel, M. and De La Rue, R. M., "Understanding the rich physics of light propagation in slow photonic crystal waveguides," SPIE Paper Number 7612-21, SPIE Photonics West, 23-28 January 2010.
28. Vlasov, Y. A., O'Boyle, M., Hamann, H. F. and McNab, S. J., "Active control of slow light on a chip with photonic crystal waveguides," Nature 438 65-69 (2005).
29. Liao., L., Samara-Rubio, D., Morse, M., Liu, A., Hodge, D., Rubin, D., Keil, U. D. and Franck, T., "High speed silicon Mach-Zehnder modulator," Opt. Express 13 (8), 3129-3135 (2005)
30. Tanabe, T., Nishiguchi, K., Kuramochi, E. and Notomi, M., "Low power and fast electro-optci silicon modulator with lateral p-i-n embedded photonic crystal nanocavity," Opt. Express 17 (25) 22505-22513 (2009).
31. Yamamoto, N., Ogawa, T. and K. Komori, "Photonic crystal directional coupler switch with small switching length and wide bandwidth," Opt. Express 14 1223 (2006).
32. Nelson, R., Leaird, D .and Weiner, A., "Programmable polarization-independent spectral phase compensation and pulse shaping," Opt. Express 11 1763-1769 (2003).
33. Waldow, M., Plotzing, T., Gottheil, M., Forst, M., Bolten, J., Wahlbrink, T. and Kurz, H., "25ps all-optical switching in oxygen implanted silicon-on-insulator microring resonator," Opt. Express 16 7693-7702 (2008).
34. Nakamura, H., Sugimoto, Y., Kanamoto, K., Ikeda, N., Tanaka, Y., Nakamura, Y., Ohkouchi, S., Watanabe, Y., Inoue, K., Ishikawa, H. and Asakawa K., "Ultra-fast photonic crystal/quantum dot all-optical switch for future photonic networks," Opt. Express 12 6606 (2004).